

Visible light photocatalytic activity of novel Ni²⁺, Cu²⁺ and VO₂ complexes derived from vanillin bidentate Schiff base ligand doped on TiO₂ nanoparticles

Morteza Dostani¹ · Ali Hossein Kianfar¹ · Mohammad Mohsen Momeni¹

Received: 29 June 2016 / Accepted: 16 August 2016 / Published online: 24 August 2016
© Springer Science+Business Media New York 2016

Abstract A new bidentate *NV*-Schiff base ligand of vanillin, (E)-4-(((2-amino-5-nitrophenyl)imino)methyl)-2-methoxyphenol, was synthesized and characterized by different spectroscopic techniques. In addition, mononuclear complexes were synthesized by treating the corresponding metal salts of Ni²⁺, Cu²⁺ and VO₂ and Schiff base ligand in methanol. The resulting complexes were characterized by FT-IR, UV-Vis and ¹H NMR techniques. The hybrids of complex/TiO₂ nanoparticles were prepared and their structure and morphology were characterized by FT-IR, XRD, TEM, SEM and solid state UV-Vis absorption. Furthermore, Kubelka-Munk transformations were used to measure the absorption curves and band gap. The photocatalytic activities of the prepared modified semiconductors were tested under visible radiation for the degradation of methylene blue in the aqueous solution. The results indicated that the incorporation of these complexes improved the activation of TiO₂ with visible light.

1 Introduction

Organic compounds containing azomethine groups can be simply manufactured by the condensation of amines and carbonyl compounds [1, 2]. Transition metal complexes derived from Schiff base ligands are one of the most comprehensively studied subjects in coordination chemistry, due to their application, example for, in anticancer

activities [3, 4], catalysis such as oxidation, reduction, epoxidation [5–8], and biological [9, 10], antibacterial, antimicrobial and antifungal agents [11–13]. Lately, extensive studies have been conducted on the photocatalytic degradation of organic dyes using Schiff base complexes because of their good photocatalytic activity [14, 15]. Although Nano-composites like cobalt ferrite nano-composite were applied to photocatalytic degradation of organic dyes in aqueous solution [16, 17] but among numerous photocatalysts, TiO₂ has been widely studied due to its strong photocatalytic activity, low cost, excellent chemical stability and non-toxicity [18–20]. TiO₂ nanoparticles have a large band gap that is the chief problem for TiO₂ nanoparticles, extremely limiting its use under visible light [21]. Recently, various researchers have attempted to decrease the band gap of TiO₂ for the absorption of visible light [22–26].

In continuation of our previous study on metal doped-TiO₂ [27], in this investigation, we synthesized and characterized bidentate Schiff base ligand and its Ni²⁺, VO₂⁺, Cu²⁺ complexes for use in photocatalytic activities. Novel bidentate ligand [(E)-4-(((2-amino-5-nitrophenyl)imino)methyl)-2-methoxyphenol; HL] was prepared by the condensation of 4-nitro-1,2-phenylenediamine and vanillin in methanol. The complexes of this ligand (2:1 ligand:metal molar ratio) with the above metals were prepared in methanol. The structure and purity of the synthesized compounds were identified by different techniques. The synthesized complexes were supported on a useful semiconductor with TiO₂ nanoparticles and calcinated by heating at 450 °C to provide M-doped TiO₂. Furthermore, photocatalytic activities of these novel semiconductor materials were investigated by the degradation of methylene blue under visible light irradiation.

✉ Ali Hossein Kianfar
akianfar@cc.iut.ac.ir; asarvestani@yahoo.com

¹ Department of Chemistry, Isfahan University of Technology, Isfahan 84156-83111, Iran

2 Experimental

2.1 Chemicals and apparatus

All of the chemicals and solvents, which were of commercially available reagent grade, and they were used without purification.

Infrared spectra were recorded as KBr discs on a FT-IR JASCO-680 spectrophotometer in the 4000–400 cm^{-1} range. UV–Vis spectra were recorded on a JASCO V-570 spectrophotometer in the range of 200–800 nm. The ^1H NMR spectra were recorded in DMSO on DPX-400 MHz FT-NMR. X-ray diffraction analysis (XRD) was carried out by using model XRD Philips X'PERT MPD, on the slope 2θ , 5–80° under the light acceleration of 40 kV/35 mA. FE-SEM was performed by using a model HITACHI (S-4160) to measure the size of nanoparticles. TEM used model Philips CM 120 with the accelerating voltage of kV150 to study the morphology of nano sized compounds and observe the size of nanoparticles.

2.2 Synthesis of H_2L

The vanillin based Schiff base ligand (HL) was synthesized by the condensation of 4-nitro-1,2-phenylenediamine and vanillin (1:1 mol ratio) in methanol. The reaction mixture was

refluxed for 8 h. Eventually, suitable crystals were formed by the slow evaporation of methanol during 48 h (Scheme 1).

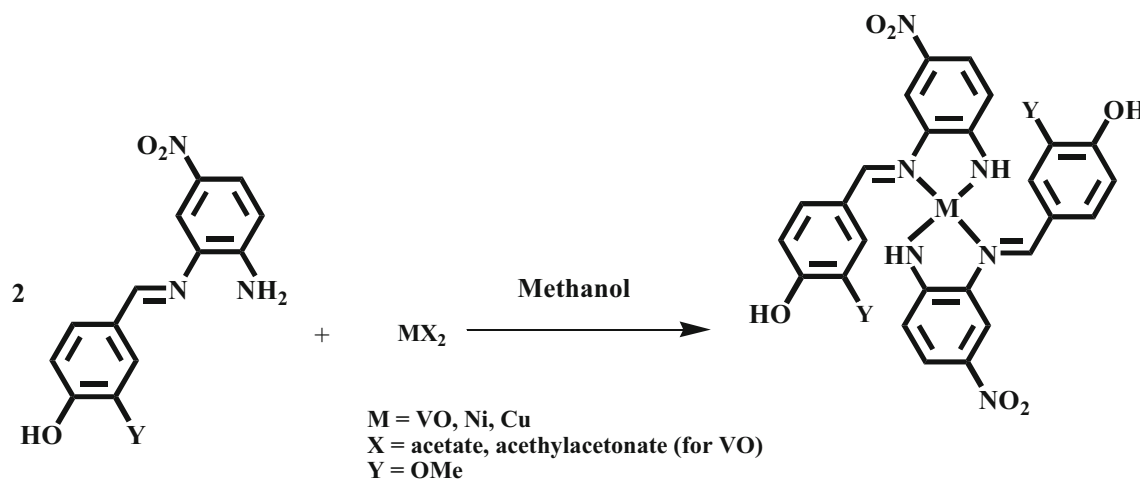
[H_2L] Yield (60 %). $\text{C}_{14}\text{H}_{13}\text{N}_3\text{O}_4$: FT-IR (KBr cm^{-1}) ν_{max} 3438 and 3336 (N–H), 1626, (C=N), 1431 (C=C), 1244 (NO_2). UV–Vis, λ_{max} (nm) (Ethanol): 209, 242, 294 (sh), 326, 397.

2.3 Synthesis of complexes

The general procedure employed for the synthesis of complexes ($[\text{NiL}_2]$, $[\text{VOL}_2]$ and $[\text{CuL}_2]$) was as follows: appropriate amounts of acetate salt (for, the acetylacetonate compound was applied) and metal were added to the 30 mL methanolic solution of HL. Then, the mixture was stirred at room temperature until the precipitate was formed. The obtained product was filtered, washed several times with methanol and then dried at 60 °C under reduced pressure (Scheme 1).

[VOL_2] Yield (75) Calc (anal) for $\text{C}_{28}\text{H}_{24}\text{N}_6\text{O}_9\text{V}$: C, 52.6(54.4); H, 3.78(3.59); N, 13.9(13.7). FT-IR (KBr cm^{-1}) ν_{max} 2940, (C–H), 1591 (C=N), 1435 (C=C), 1213 (NO_2); UV–Vis, λ_{max} (nm) (Ethanol): 351, 287, 236, 212.

[CuL_2] Yield (85 %). Calc (anal) for $\text{C}_{28}\text{H}_{24}\text{N}_6\text{O}_8\text{Cu}$: C, 53.27(54.98); H, 3.80(3.65); N, 13.31(13.56). FT-IR (KBr cm^{-1}) ν_{max} 2932 (C–H), 1596 (C=N), 1428 (C=C), 1222 (NO_2); UV–Vis, λ_{max} (nm) (Ethanol): 353, 287, 234, 207.



Scheme 1 The structure of Schiff base ligand and its complexes

Table 1 Characteristic IR bands (cm^{-1}) of the ligand and its complexes

Compound	$\nu\text{N-H}$ (cm^{-1})	$\nu\text{C=N}$ (cm^{-1})	$\nu\text{C=C}$ (cm^{-1})	$\nu\text{N-O}$ (cm^{-1})	$\nu\text{V-O}$ (cm^{-1})
H_2L	3438, 3336	1626	1431	1244	–
VOL_2	3100	1591	1435	1213	978
NiL_2	3106	1596	1466	1221	–
CuL_2	3098	1596	1428	1222	–

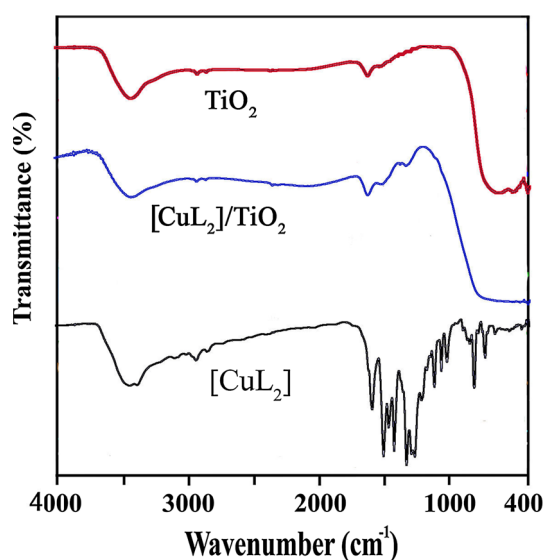


Fig. 1 The FT-IR spectra of $[\text{CuL}_2]$, $[\text{CuL}_2]/\text{TiO}_2$ and TiO_2

Table 2 UV-Vis spectral data (nm) for the ligand and its complexes

Compound	λ_1	λ_2	λ_3	λ_4	λ_5
H_2L	378	322	292(sh)	240	207
VOL_2	352	–	287	237	212
NiL_2	353	–	287	234	210
CuL_2	363	–	288	236	209

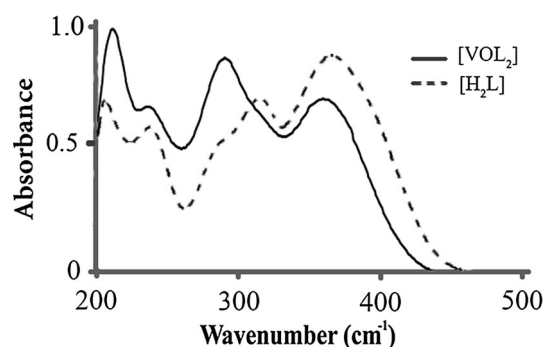


Fig. 2 The UV spectrum of ligand and $[\text{VOL}_2]$

$[\text{NiL}_2]$ Yield (80 %). Calc (anal) for $\text{C}_{28}\text{H}_{24}\text{N}_6\text{O}_8\text{Ni}$: C, 52.87(54.68); H, 3.77(3.56); N, 13.21(13.81): FT-IR (KBr cm^{-1}) ν_{max} 3053, 2914 (C–H), 1592, (C=N), 1437 (C=C), 1221 (NO_2); UV-Vis, λ_{max} (nm) (Ethanol): 363, 288, 236, 210.

2.4 Synthesis of $[\text{ML}_2]/\text{TiO}_2$

0.1 g of $[\text{ML}_2]$ complexes (M=Ni, VO, Cu) was dissolved in DMF and added to a beaker including 0.8 g TiO_2 nanoparticles. The reaction was refluxed for 5 h. Finally,

the mixture was filtered and washed with methanol. The solids were dried for 2 h at 60 °C before characterization.

2.5 Synthesis of NiO, CuO, and $\text{V}_2\text{O}_5/\text{TiO}_2$ nano metal mixed oxide

M-doped TiO_2 nanohybrids were prepared by the calcination of $[\text{ML}_2]/\text{TiO}_2$ at temperatures up to 450 °C for 4 h in an oven.

2.6 Photocatalytic experiments

Photocatalytic activities of the prepared samples were evaluated by the degradation of the aqueous methylene blue (MB) as the model pollutant under xenon lamp irradiation. The photocatalytic reaction was carried in a single-compartment cylindrical quartz reactor. A 200 W xenon lamp A 200 W xenon lamp with the luminous intensity of 100 mW/cm^2 was used as a light source. The actual experiments were performed at room temperature. The initial concentrations of methylene blue, 2 mg/L and 0.1 g as-prepared photocatalysts were mixed with a magnetic stirrer. Prior to illumination, to ensure the establishment of an adsorption-desorption equilibrium between the photocatalyst and methylene blue, the solution was magnetically stirred for 2 h in the dark. Then it was exposed to light irradiation under magnetic stirring for 300 min. At certain time intervals, specific amount a of the solution was withdrawn and photocatalysts were separated by centrifuging; then changes in the concentration of MB were observed using a UV-Vis spectrophotometer.

3 Results and discussion

3.1 IR characteristics

The IR spectra of ligand and the synthesized complexes are listed in Table 1. The spectrum of the free Schiff base ligand displayed the peak of azomethine group $-\text{CH}=\text{N}$ at 1626 cm^{-1} , which was shifted to the lower frequencies in the spectra of all complexes within the range of 1596 – 1591 cm^{-1} . This showed that the lone electron pair of the nitrogen atom of $-\text{CH}=\text{N}$ was coordinated with metal ions [28].

In the IR spectra of all complexes, peaks at 3438 and 3336 cm^{-1} of NH_2 in the free Schiff base ligand were changed to NH and shifted to the lower frequencies, indicating that the nitrogen atom was coordinated with metal ions as $-\text{NH}$ functional group.

The IR spectra of pure TiO_2 nanoparticles, $[\text{CuL}_2]$ complex and the modified $\text{TiO}_2/\text{CuL}_2$ are shown in Fig. 1. Pure TiO_2 showed strong absorption bands at 415, 510 and

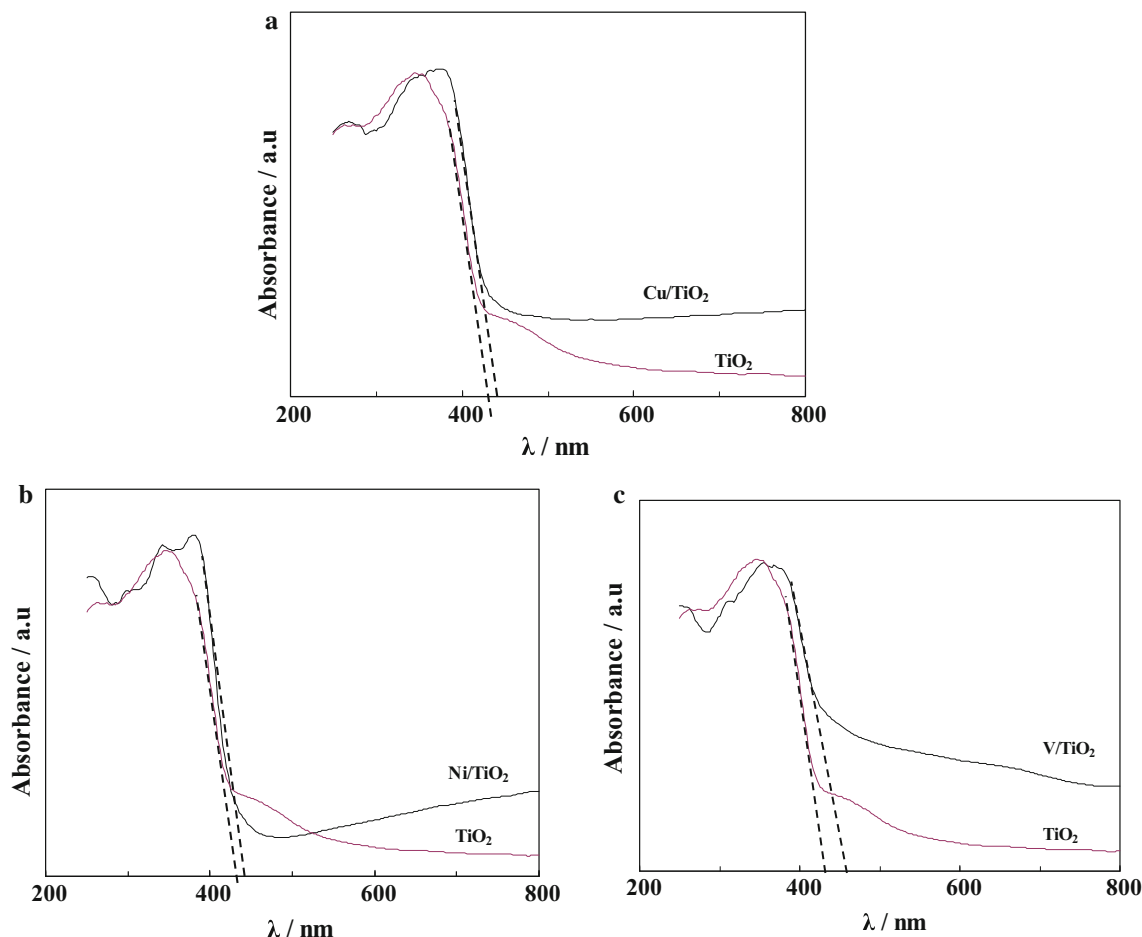


Fig. 3 Diffuse reflectance spectra (DRS) of different samples; **a** TiO₂ and Cu/TiO₂, **b** TiO₂ and Ni/TiO₂ and **c** TiO₂ and V/TiO₂

626 cm⁻¹ which were related to the vibration of the Ti–O and O–Ti–O bonds [29]. Also, the notable peaks observed in the regions 1629 and 3433 cm⁻¹ were related to the vibration of hydroxyl groups associated by water on the surface of TiO₂.

The infrared spectrum of the modified semiconductors with [ML₂] confirmed that the complexes were absorbed on the surface of TiO₂. The new weak peaks obtained at 1517 and 1336 cm⁻¹ could be related to the functional group of complex.

3.2 Electronic spectra

The UV–Vis spectral data of the ligand and synthesized complexes are listed in the experimental section and the results are summarized in Table 2. The electronic spectral data of the free Schiff base ligand was obtained in ethanol with five absorption bands, i.e., 209, 242, 294 (sh), 326 and 397 nm. The bands at 209, 242 and 294 nm were related to the $\pi \rightarrow \pi^*$ transition of the aromatic ring [30]. The

transition bands at 326 and 397 nm included $n \rightarrow \pi^*$ (N–H) and $\pi \rightarrow \pi^*$ (–C = N) transitions, respectively. Due to the coordination of the ligand, the last transitions were shifted to higher energies. On the other hand, the $\pi \rightarrow \pi^*$ transition of aromatic rings with a slightly change appeared in the same place with the free ligand (Fig. 2) [31].

3.3 UV–Vis diffuse reflectance spectra

Figure 3 represents the UV–Vis of the undoped and doped TiO₂ samples. The results indicated that optical reflection edge was obviously shifted to the visible light range with transition metal additives. The observed red shifts for the metal-doped TiO₂ catalysts indicated that the band gap energy of samples was decreased gradually. The calculated band gap energies from Tauc plot for different samples were 2.81, 2.85 and 2.69 eV for different types of promoters, namely, Cu, Ni and VO, respectively. As a result, the band gap energies of the doped TiO₂ were narrower than those of the non-doped TiO₂.

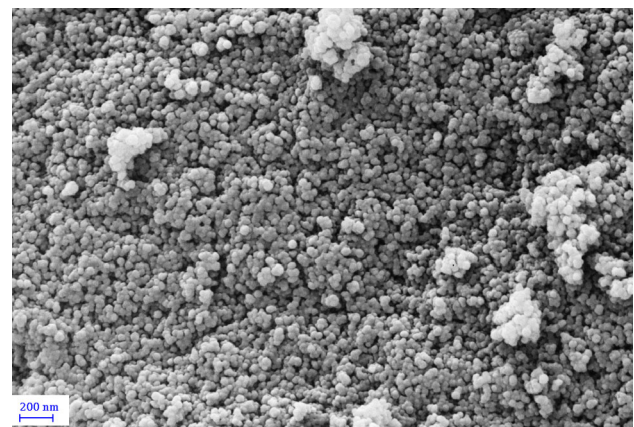
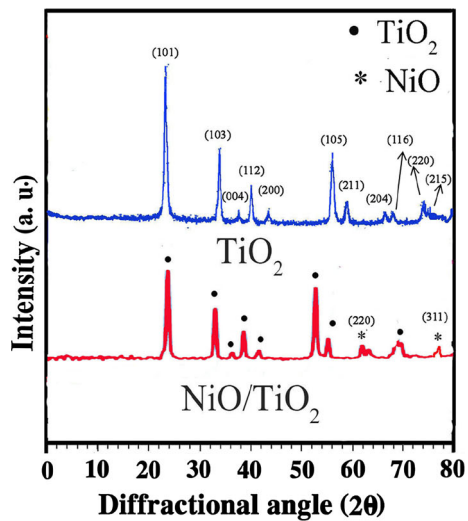


Fig. 5 SEM of [VOL₂]/TiO₂

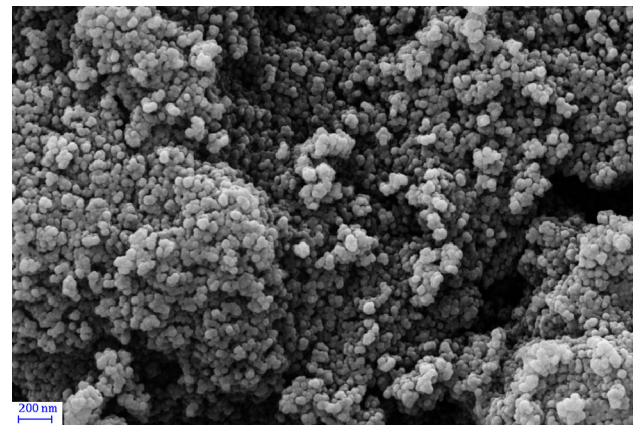
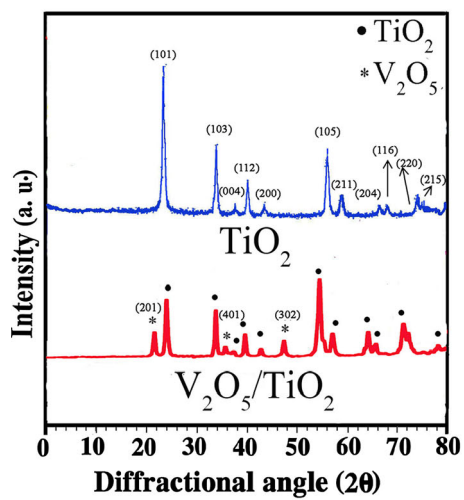


Fig. 6 SEM of V₂O₅/TiO₂

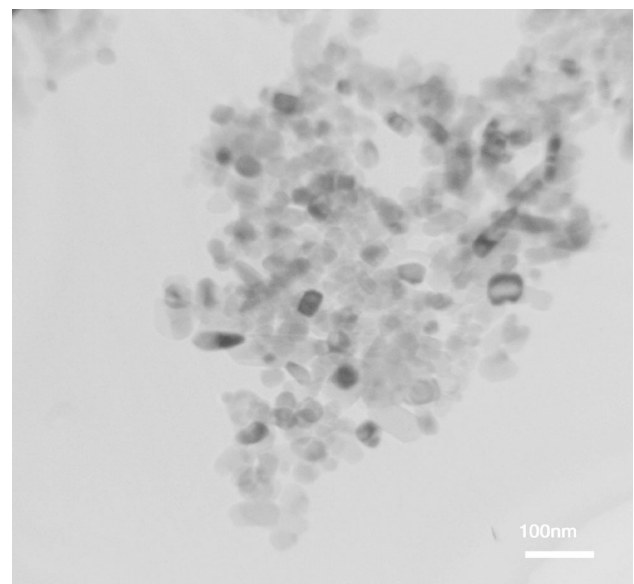
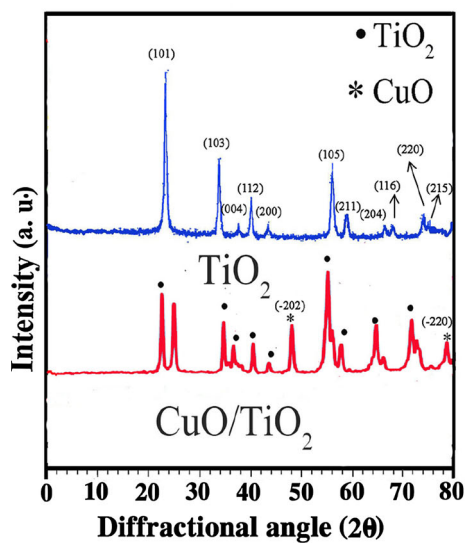


Fig. 7 TEM of V₂O₅/TiO₂

Fig. 4 The XRD TiO₂ and MO_x/TiO₂

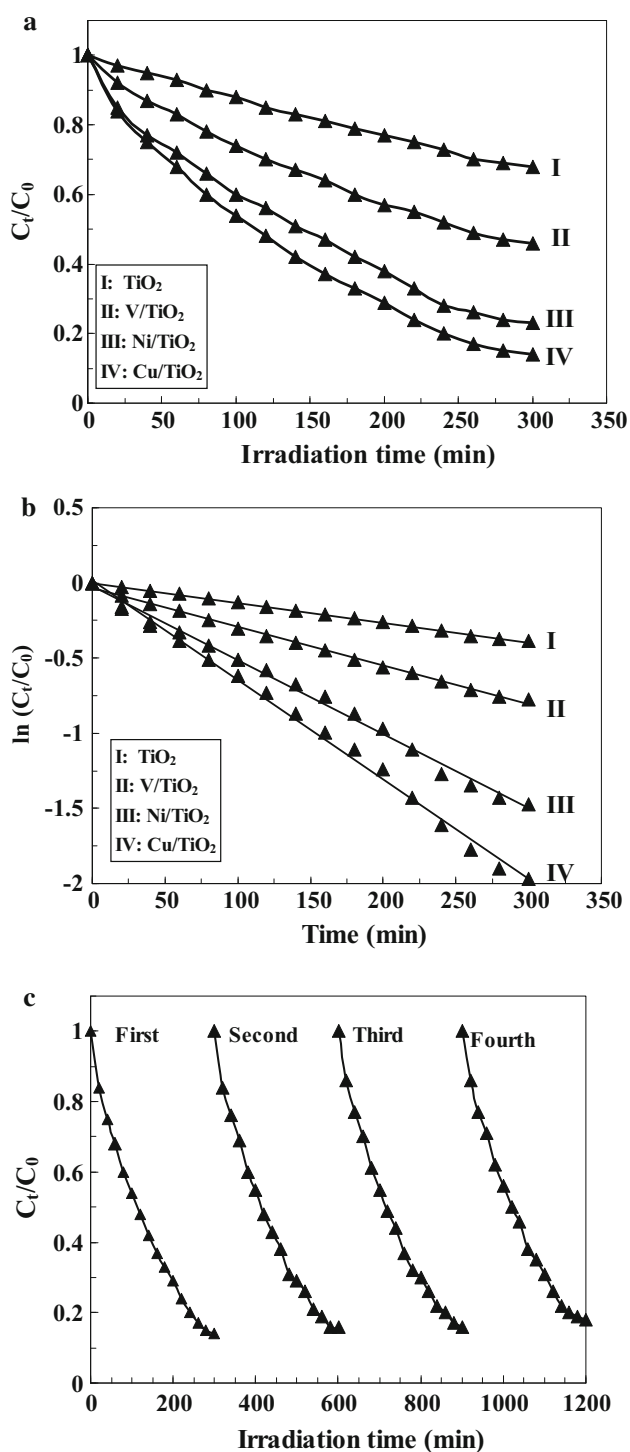


Fig. 8 a The photocatalytic degradation of MB over the different samples under xenon light irradiation. b $\ln(C_t/C_0)$ versus irradiation time plot. c Photocatalyst stability test of Cu/TiO_2 sample

3.4 X-ray diffraction

The XRD patterns of pure TiO_2 and $[\text{ML}_2]/\text{TiO}_2$ after calcination (MO_x/TiO_2) at 450°C are shown in Fig. 4.

According to the XRD pattern of TiO_2 nanoparticles [32], the obvious peaks on 25(101), 35(103), 36(004), 38(112), 48(200), 53(105), 55(211), 62(204), 68(116), 70(220) and 75(215) confirmed the anatase phase (JCPDS no. 01-0841283). According to the XRD patterns of MO_x/TiO_2 , the important peaks of TiO_2 and the peaks related to MO metal oxide could be obviously observed from the MO_x/TiO_2 spectrum, showing the presence of metal oxides in the nanocomposite [NiO (JCPDS no. 00-047-1049), V_2O_5 (JCPDS no. 00-041-1426) and CuO (JCPDS no. 00-045-0937)].

3.5 Morphology analysis

To further study the morphology of mixed nanoparticles, the SEM and TEM were implemented. SEM images for $[\text{VOL}_2]/\text{TiO}_2$ (Fig. 5) and its calcinated form (Fig. 6) displayed the good dispersion of the complex on TiO_2 surface; according to the SEM images, there were nano size spherical particles in the range of 40–50 nm.

TEM analysis for $\text{V}_2\text{O}_5/\text{TiO}_2$ (Fig. 7) showed a suitable dispersal followed by the aggregation of spherical TiO_2 particles with the size of about 40 nm.

3.6 Photocatalytic studies

The photocatalytic activity of the prepared samples was followed by the degradation of methylene blue as a function of irradiation time. To get the response of photocatalytic activities of bare TiO_2 , V/TiO_2 , Ni/TiO_2 and Cu/TiO_2 samples, absorption spectra of the exposed samples at various time intervals were recorded and the rate of color degradation was observed in terms of the change in the intensity at λ_{max} of dye. The photo degradation yield can be defined as:

$$\text{Photodegradation yield (\%)} = [(C_0 - C)/C_0] \times 100, \quad (1)$$

where C_0 and C are the initial concentration and the concentration of dyes after photodegradation, under visible light irradiation, and at various time intervals, respectively. In order to obtain the real photodegradation yield, dye concentration should not be decreased to avoid adsorption and direct photolysis. The photocatalysis results indicated that the photocatalytic process was very effective in the removal of methylene blue. Figure 8a shows the photodegradation rate of MB under Xe lamp light in the presence of different samples. It can be seen that the photocatalytic degradation efficiencies of MB for 300 min over Cu/TiO_2 , Ni/TiO_2 , V/TiO_2 and TiO_2 were 86, 77, 54 and 32 %, respectively, in which Cu/TiO_2 sample gave the highest removal rate. Photocatalytic reactions kinetics can

Table 3 The apparent first-order rate constant (k) of photocatalytic degradation of methylene blue for different samples

Samples	Apparent rate constant, k (min^{-1})	Correlation coefficient, R^2
TiO ₂	1.30×10^{-2}	0.9983
V/TiO ₂	2.60×10^{-2}	0.9968
Ni/TiO ₂	4.90×10^{-2}	0.9936
Cu/TiO ₂	6.60×10^{-2}	0.9948

be expressed by the Langmuir–Hinshelwood (L–H) model [33–36]:

$$\ln(C_0/C) = k_{\text{app}}t \quad (2)$$

where k_{app} is the apparent pseudo first order reaction rate constant and t is the reaction time. A plot of $\ln(C_0/C)$ versus t can yield a slope of k_{app} . The calculated k_{app} and correlation coefficients corresponding to Fig. 8b are listed in Table 3. Among all the samples, Cu/TiO₂ sample demonstrated relatively higher rate constants than the rest of samples for MB degradation $6.60 \times 10^{-2} \text{ min}^{-1}$ was calculated as the maximum reaction rate constant for Cu/TiO₂, confirming that this catalyst was successful in MB degradation and Cu doping enhanced the photocatalytic activity. The photocatalytic performances of different samples were in the following order:

$$\text{Cu/TiO}_2 > \text{Ni/TiO}_2 > \text{V/TiO}_2 > \text{TiO}_2$$

For the pure TiO₂, the photocatalytic activity was the lowest and degradation of MB was only 32 % for 300 min; this was because this sample could only absorb UV light, not the visible light. The higher photocatalytic activity of the doped samples could be attributed to the combined effect of several factors: the type of doped material and increased light-harvesting ability (the capability of absorbing visible light and higher light absorption, as compared to the pure TiO₂).

The stability of a photocatalyst is also important for its practical application, so that it can be regenerated and reused. We investigated the cyclic stability of Cu/TiO₂ sample by monitoring the catalytic activity during the successive cycles of use. As shown in Fig. 8c, after a four-cycle experiment, this catalyst exhibited a similar catalytic performance without significant deactivation, thereby revealing its high stability after multiple reuses.

4 Conclusion

The present work was a research on synthesis, characterization and photo-catalytic activities of Schiff base complexes. In this article, a bidentate Schiff base ligand and its nickel, copper and vanadyl metal complexes were synthesized. In order to prepare well-shaped nano structure

compounds for photo-catalysis reactions, the synthesized complexes were applied as solids support for TiO₂ nano metal oxide to get better results in the photo-catalysis process and a series of transition metal doped (V, Ni and Cu) TiO₂ photocatalysts were prepared. The optical reflection edge was obviously shifted to the visible light range with these transition metal additives. The band gap energies of the doped TiO₂ samples were considerably narrower than those of the pure TiO₂. The results showed that loading titania with different transition metal elements had a significant influence on the catalytic activity during dye degradation reactions. Among all the catalysts, Cu/TiO₂ sample exhibited the highest photocatalytic activity for methylene blue degradation owing to the low band gap energy and delayed electron–hole recombination.

5 Acknowledgments

We wish to express our gratitude to the Research Affairs Division at Isfahan University of Technology (IUT), Isfahan, for the partial financial support.

References

1. S.C. Bell, G.L. Conklin, S.J. Childress, *J. Am. Chem. Soc.* **85**, 2867 (1963)
2. J. Kjeld, C. van Bommel, W. Verboom, H. Kooijman, A.L. Spek, N.D. Reinhoudt, *Inorg. Chem.* **37**, 4197 (1998)
3. J. Zuo, C.F. Bi, Y.H. Fan, D. Buac, C. Nardon et al., *J. Inorg. Biochem.* **118**, 83 (2013)
4. B.S. Creaven, B. Duff, D.A. Egan, K. Kavanagh et al., *Inorg. Chim. Acta Part A* **363**, 4048 (2010)
5. M. Moghadam, V. Mirkhani, S. Tangestaninejad, I. Mohammadpoor-Baltork, A.A. Abbasi-Larki, *Appl. Catal. A* **349**, 177 (2008)
6. P.G. Cozzi, *Chem. Soc. Rev.* **33**, 410 (2004)
7. Z. Dong, X. Le, X. Li, W. Zhang, C. Dong, J. Ma, *Appl. Catal. B Environ.* **158–159**, 129 (2014)
8. M.E. Davis, *Nature* **417**, 813 (2002)
9. M. Sahin, N. Kocak, D. Erdenay, U. Arslan, *Spectrochim. Acta, Part A* **103**, 400 (2013)
10. M.A. Phaniband, S.D. Dhumwad, *Transit. Met. Chem.* **32**, 1117 (2007)
11. J.R. Anaconda, N. Noriega, J. Camus, *Spectrochim. Acta, Part A* **137**, 16 (2015)
12. K.T. Joshi, A.M. Pancholi, K.S. Pandya, K.K. Singh, A.S. Thakkar, *Asian J. Chem.* **22**, 7706 (2010)
13. S.A. Patil, C.T. Prabhakara, B.M. Halasangi, S.S. Toragalmath, P.S. Badami, *Spectrochim. Acta, Part A* **137**, 641 (2015)

14. S. Wang, L.N. Bai, H.M. Sun, Q. Jiang, J.S. Lian, *Power Technol.* **244**, 9 (2013)
15. N.B. Gopal Reddy, P. Murali Krishna, N. Kottam, *Spectrochim. Acta, Part A* **137**, 371 (2015)
16. M.H. Habibi, J. Parhizkar, *Spectrochim. Acta, Part A* **150**, 879 (2015)
17. M.H. Habibi, Z. Rezbani, *Spectrochim. Acta, Part A* **147**, 173 (2015)
18. A. Fujishima, X. Zhang, D.A. Tryk, *Surf. Sci. Rep.* **63**, 515 (2008)
19. A.D. Paola, E. García-López, G. Marci, L. Palmisano, *J. Hazard. Mater.* **211–212**, 3 (2012)
20. Y.Q. Wang, R.R. Zhang, J.B. Li, L.L. Li, S.W. Lin, *Nanoscale Res. Lett.* **9**, 46 (2014)
21. B. Ohtani, *Chem. Lett.* **37**, 216 (2008)
22. M.H. Habibi, M.H. Rahmati, *Spectrochim. Acta, Part A* **133**, 13 (2014)
23. G. Fan, J. Tong, F. Li, *Ind. Eng. Chem. Res.* **51**, 13639 (2012)
24. K.S.U. Mhan, M. Al-Shahry, W.B. Ingler, *Science* **297**, 2243 (2002)
25. S. Song, J. Tu, Z. He, F. Hong, W. Liu, J. Chen, *Appl. Catal. A* **378**, 169 (2010)
26. Y. Li, X. Zhou, X. Hu, X. Zhao, P. Fang, *J. Phys. Chem. C* **113**, 16188 (2009)
27. A.H. Kianfar, P. Dehghani, M.M. Momeni, *Mater. Sci. Mater. Electron.* **27**, 3368 (2016)
28. A.H. Kianfar, L. Keramat, M. Dostani, M. Shamsipur, M. Roushani, F. Nikpour, *Spectrochim. Acta Part A* **77**, 424 (2010)
29. X.T. Yoko, K. Kamiya, K. Tanaka, *J. Mater. Sci.* **25**, 3922 (1990)
30. A.A.A. Emara, *Spectrochim. Acta, Part A* **77**, 117 (2010)
31. M.S. Refat, I.M. El-Deen, H.K. Ibrahim, S. El-Ghool, *Spectrochim. Acta, Part A* **65**, 1208 (2006)
32. J. Yan, G. Wu, N. Guan, L. Li, Z. Li, X. Cao, *Phys. Chem. Chem. Phys.* **15**, 10978 (2013)
33. M.M. Momeni, Y. Ghayeb, *J. Mater. Sci.: Mater. Electron.* **27**, 1062 (2016)
34. M.M. Momeni, Y. Ghayeb, *Ceramic. Int.* **42**, 7014 (2016)
35. M.M. Momeni, Y. Ghayeb, *J. Mol. Catal. A: Chem.* **417**, 107 (2016)
36. A.K.L. Sajjad, S. Shamaila, B. Tian, F. Chen, J. Zhang, *J. Hazard. Mater.* **177**, 781 (2010)